



# Effect of Tool Rotation Speed on Microstructure and Microhardness of Friction-Stir-Processed Cold-Sprayed SiCp/Al5056 Composite Coating

Chunjie Huang, Wenya Li, Zhihan Zhang, Marie-pierre Planche, Hanlin Liao, and Ghislain Montavon

(Submitted January 11, 2016; in revised form June 15, 2016)

SiC-particle-reinforced Al5056-matrix composite coatings were deposited onto Al2024 substrates by cold spraying using a powder mixture having 15 vol.% SiC. To investigate the effects of friction stir processing (FSP) parameters on the microstructure and microhardness of the as-sprayed coating, the as-sprayed composite coating was then subjected to FSP using a stir tool having a threaded pin with rotation speed of 600 rpm and 1400 rpm. Results showed that the coatings presented Al and SiC phases before and after FSP treatment, and no other diffraction peaks were detected. Fine grains were produced in the Al5056 matrix due to severe plastic deformation during FSP, and the refined SiC particles exhibited a homogeneous distribution in the FSPed coating. In addition, an evident reduction of porosity (from 0.36% to 0.08% at 600 rpm or 0.09% at 1400 rpm) occurred, and a dramatic size reduction of the reinforcement from 12.5  $\mu\text{m}$  to 6.5  $\mu\text{m}$  at 600 rpm or 7.0  $\mu\text{m}$  at 1400 rpm was achieved. Nevertheless, the microhardness profile presented general softening and a decrease from 143.9 HV to about 110 HV.

**Keywords** cold spraying, friction stir processing, microstructure, microhardness, SiCp/Al5056 composite coating

## 1. Introduction

Particle-reinforced metal-matrix composite (PRMMC) coatings combine the properties of metals (high strength and toughness) with those of ceramics (excellent wear and corrosion resistance, and chemical stability), which increases the service life of components. However, it is difficult to fabricate high-performance PRMMC coatings by conventional means, especially with high volume fraction of ceramics.

Cold spraying (CS), as a solid-state process, has shown many advantages (Ref 1-3), such as low processing temperature and high deposition efficiency, in producing PRMMC coatings (e.g., Al and its alloys, Ni and its alloys,

Cu-based coatings, and other metal-ceramic coatings) compared with traditional thermal spraying, so use of CS to form PRMMC coatings has become a hot research topic (Ref 4-9). As reported by Moridi et al. (Ref 1), production of PRMMC coatings by CS could be very useful, as such composites enable tailoring of physical and mechanical properties. In addition, those authors also presented that the presence of reinforcement particles as well as their size and size distribution would have a significant influence on the coating hardness. However, according to Ref 5, 6, 8, the distribution and content of reinforcement could not be effectively controlled within as-sprayed PRMMC coatings, and in Li et al.'s work (Ref 6), the coating compactness and bonding strength could be effectively enhanced via postspray heat treatment (PSHT). However, it had little effect on the size, morphology, and distribution of the reinforcement. Against this background, it is interesting to consider modification of the microstructure and redistribution and refinement of the reinforcement in as-sprayed PRMMC coatings by PSHT.

Recently, much attention has been paid to a new solid-state processing technique, i.e., friction stir processing (FSP) (Ref 10), an adaptation of friction stir welding (FSW) (Ref 11), which has now matured into an important surface modification technique. In this case, a rotating tool with a pin and shoulder is inserted into a single piece of material for localized microstructural modification; For example, Ma et al. (Ref 12) and Sharma et al. (Ref 13) indicated that FSP was successful for producing fine-grained structures (Ref 14) and surface nanocomposite layers (Ref 15), modifying the microstructure of materials (Ref 7, 16), and synthesizing intermetallic compounds

**Chunjie Huang**, IRTES EA7274, Université Bourgogne Franche-Comté, UTBM, Site de Sévenans, 90010 Belfort Cedex, France; and State Key Laboratory of Solidification Processing, Northwestern Polytechnical University, Xian 710072, People's Republic of China; **Wenya Li** and **Zhihan Zhang**, State Key Laboratory of Solidification Processing, Northwestern Polytechnical University, Xian 710072, People's Republic of China; and **Marie-pierre Planche**, **Hanlin Liao**, and **Ghislain Montavon**, IRTES EA7274, Université Bourgogne Franche-Comté, UTBM, Site de Sévenans, 90010 Belfort Cedex, France. Contact e-mail: liwy@nwpu.edu.cn.

in situ (Ref 17), and demonstrated that FSP is a very effective solid-state processing technique that could provide localized modification and control of microstructure in the surface layers of metallic components (Ref 12). In addition, Salih et al. (Ref 18) further presented state-of-the-art joining of particle-reinforced aluminum-matrix composites (PRAMC) by FSW, including the weldability of AMCs, their macro- and microstructure, and the mechanical properties of joints, proving that FSW is a promising approach for joining AMCs. In addition, Morisada et al. (Ref 19) applied FSP to modify thermally sprayed WC-CrC-Ni coating by using a sintered cemented carbide (WC-Co) tool, finding that defects in the cemented carbide layer disappeared while the hardness increased to 2000 HV, about 1.5 times higher than that of the as-sprayed cemented carbide layer. Hodder et al. (Ref 7) implemented FSP on cold-sprayed  $\text{Al}_2\text{O}_3/\text{Al}$  coating using a flat cylindrical tool (Ref 20), finding that FSP at a higher rotation speed was effective for dispersing  $\text{Al}_2\text{O}_3$  particles and decreasing their mean free path. It was also suggested that the microhardness was greatly improved by redistribution and refinement of  $\text{Al}_2\text{O}_3$ .

Based on the above discussion of applications of the FSW and FSP techniques, it can be considered that implementation of FSP on cold-sprayed SiCp/Al5056 composite coating is feasible, as proven by our preliminary study (Ref 21). Therefore, the present study focused on investigation of the influence of tool rotation speed on the microstructure and microhardness of cold-sprayed PRAMC coating.

## 2. Experimental

The feedstock powder was a mixture of Al5056 powder as matrix with 15% volume fraction of SiC powder as reinforcement. The Al5056 powder had spherical shape (Fig. 1a) with size distribution ranging from 8.7 to 39.4  $\mu\text{m}$  and average size of 19.6  $\mu\text{m}$ . The SiC powder had irregular morphology (Fig. 1b) with size distribution ranging from 48.3 to 92.6  $\mu\text{m}$  and average size of 66.9  $\mu\text{m}$ . Al2024 plates (50 × 50  $\text{mm}^2$ ) were used as substrate. To enhance

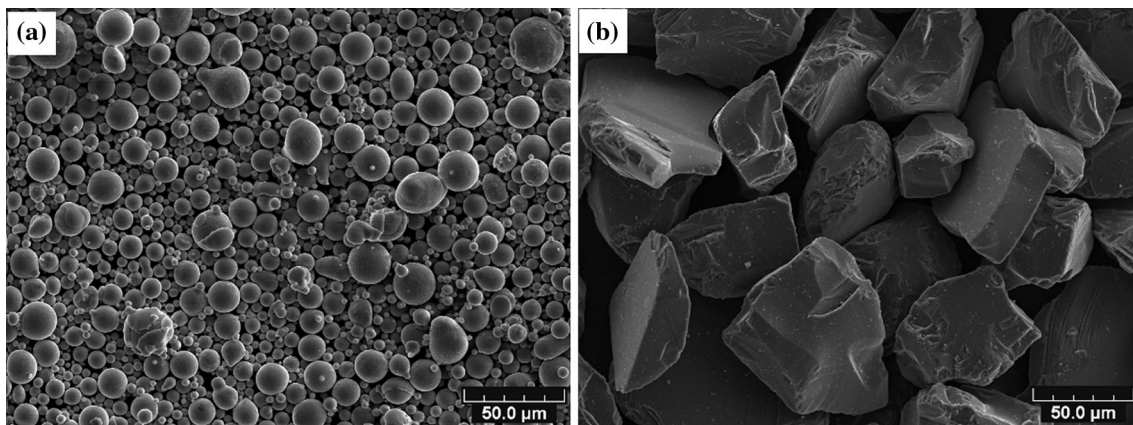


**Fig. 1** Morphology of (a) Al5056 and (b) SiC powders

adhesion between the substrate and coating, the substrate was sand-blasted using alumina grits prior to spraying, then rinsed in an ultrasonic bath with acetone to remove adsorbed species and residual alumina.

SiCp/Al5056 coatings were then deposited onto substrates using CS. A commercial spray gun (Kinetics<sup>®</sup> 3000, CGT GmbH, Germany) with a converging-diverging nozzle was used to spray the coatings. High-pressure compressed air was used as driving gas at inlet pressure of 2.6 MPa and temperature of about 500 °C. Argon was used as powder carrier gas at pressure of 2.8 MPa. The standoff distance was fixed at 30 mm.

The as-sprayed composite coating was then FSPed (parallel to the spraying direction) with one pass on a commercial FSW machine (FSW-RL31-010, Beijing FSW Technology Co. Ltd., PR China) at welding speed of 100 mm/min and rotation speed of 600 or 1400 rpm. The stir tool was characterized by a threaded pin with 3.4 mm root diameter and 2.9 mm length, as well as a concave shoulder of 10 mm diameter. The tool was tilted 2.5° during FSP. The stir zone was cross-sectioned perpendicular to the processing direction for metallographic analysis, as marked by the black frame in Fig. 2.

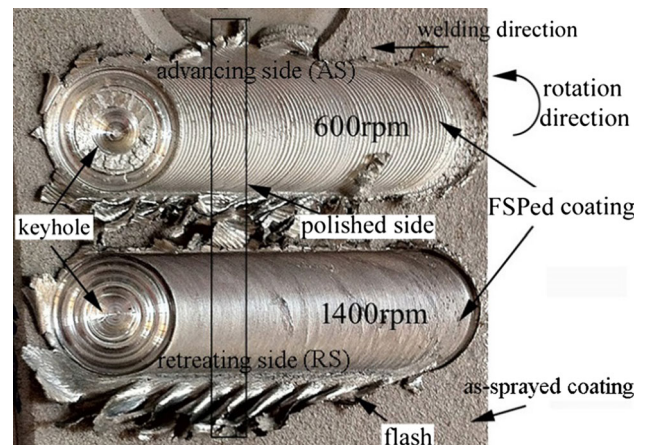


**Fig. 2** General morphologies of as-sprayed SiCp/Al5056 coating after FSP at 600 rpm (upper) or 1400 rpm (lower)



Optical microscopy (OM; Nikon, Japan) and scanning electron microscopy (SEM; JSM 5800LV, Japan) were used for microstructural observations. The particle size distribution was measured by laser diffractometry (Mastersizer 2000, Malvern Instruments Ltd., UK). The phase composition of the coatings before and after FSP treatment was determined by x-ray diffraction (XRD) analysis (X'Pert diffractometer, Philips, The Netherlands). The coating porosity and reinforcement size were estimated by analysis of metallurgical images using at least ten cross-sectional SEM micrographs. Before analysis, the metallographic specimens were etched using Keller's reagent. Microhardness measurements were carried out using a Vickers hardness indenter (Leitz, Germany) with load of 300 g and dwell time of 15 s in the stir zone.

### 3. Results and Discussion

#### 3.1 Macrostructure of FSPed Coating

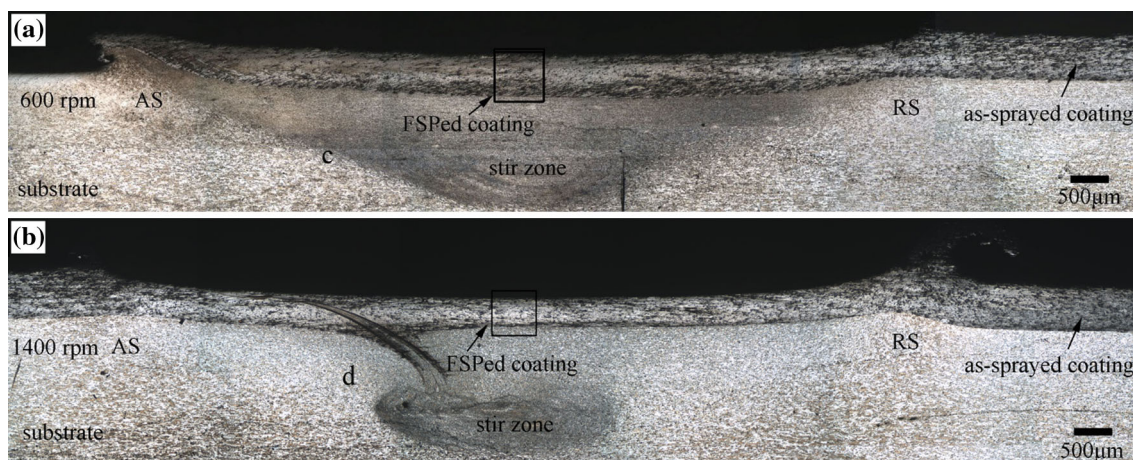
Figure 2 shows the general morphology of welds on the as-sprayed coating for the rotation speeds of 600 and 1400 rpm. This figure indicates that FSP was successfully implemented on the as-sprayed SiCp/Al5056 coating without detachment of the coating from the substrate. For the weld at 600 rpm, the inadequate rotation speed resulted in a coarse surface because of plastic deformation under the relatively low heat input. It also demonstrates that a relatively higher rotation speed is more effective for producing a smooth surface. Favorable processing parameter values should be determined according to the microstructure and property of the FSPed coatings. Moreover, there is no obvious evidence for occurrence of defects or voids for the two welds. Similar to the FSW process, heavy flash occurred at the retreating side (RS) and a keyhole was present after pulling out the tool (Ref 22, 23).

Figure 3(a), (b) shows the cross-sectional OM morphologies of the FSPed coatings at 600 and 1400 rpm,

respectively. It can be clearly seen that the coating FSPed at 600 rpm showed comparable thickness (632  $\mu\text{m}$ ) to the as-sprayed coating (665  $\mu\text{m}$ ), while the coating FSPed at 1400 rpm presented a relatively lower thickness (415  $\mu\text{m}$ ) with larger flash on the RS. Observing the interfaces between the FSPed coating and the substrate, it was found that an apparent boundary was still present. However, improvement of the compactness at the interface during FSP might play a considerable role in enhancing the coating bonding strength. In addition, it is worth noting that the SiC particles were not incorporated into the substrate and the stirred zones at 600 and 1400 rpm presented basin and elliptical profiles (Ref 22), respectively. Similar to FSW, the stirred zones within the Al2024 substrate consisted of fine equiaxed recrystallized grains due to the intensive thermomechanical effect during FSP, thus greatly improving the composite coating and substrate (Ref 23).

#### 3.2 Microstructure Characterization

A typical cross-sectional SEM micrograph of the as-sprayed SiCp/Al5056 coating is presented in Fig. 4(a). It seems that the as-sprayed coating had dense structure because of the higher density of SiC than Al5056, enhancing the kinetic impact process during codeposition of metal and ceramic (Ref 6, 7). When observed at higher magnification, as shown in Fig. 4b, some obvious pores were found at multiparticle boundaries due to insufficient deformation of Al5056 particles, and the porosity of the as-sprayed coating was  $0.36 \pm 0.12\%$ . In addition, some obvious cracks and interlocking were observed at interfaces of particles, suggesting that mechanical bonding seems to be the main bonding mechanism between the Al5056 particles. The interfaces between particles and grain boundaries within a particle were obvious after etching. Furthermore, the SiC particles were well embedded in Al5056 particles, and relatively uniformly dispersed in the Al5056 matrix with average size of 12.5  $\mu\text{m}$ , as shown in Fig. 5(a), much smaller than the



**Fig. 3** Cross-sectional OM macrostructures of coatings FSPed at rotation speed of 600 rpm (a) and 1400 rpm (b), showing stirred coating and as-sprayed coating

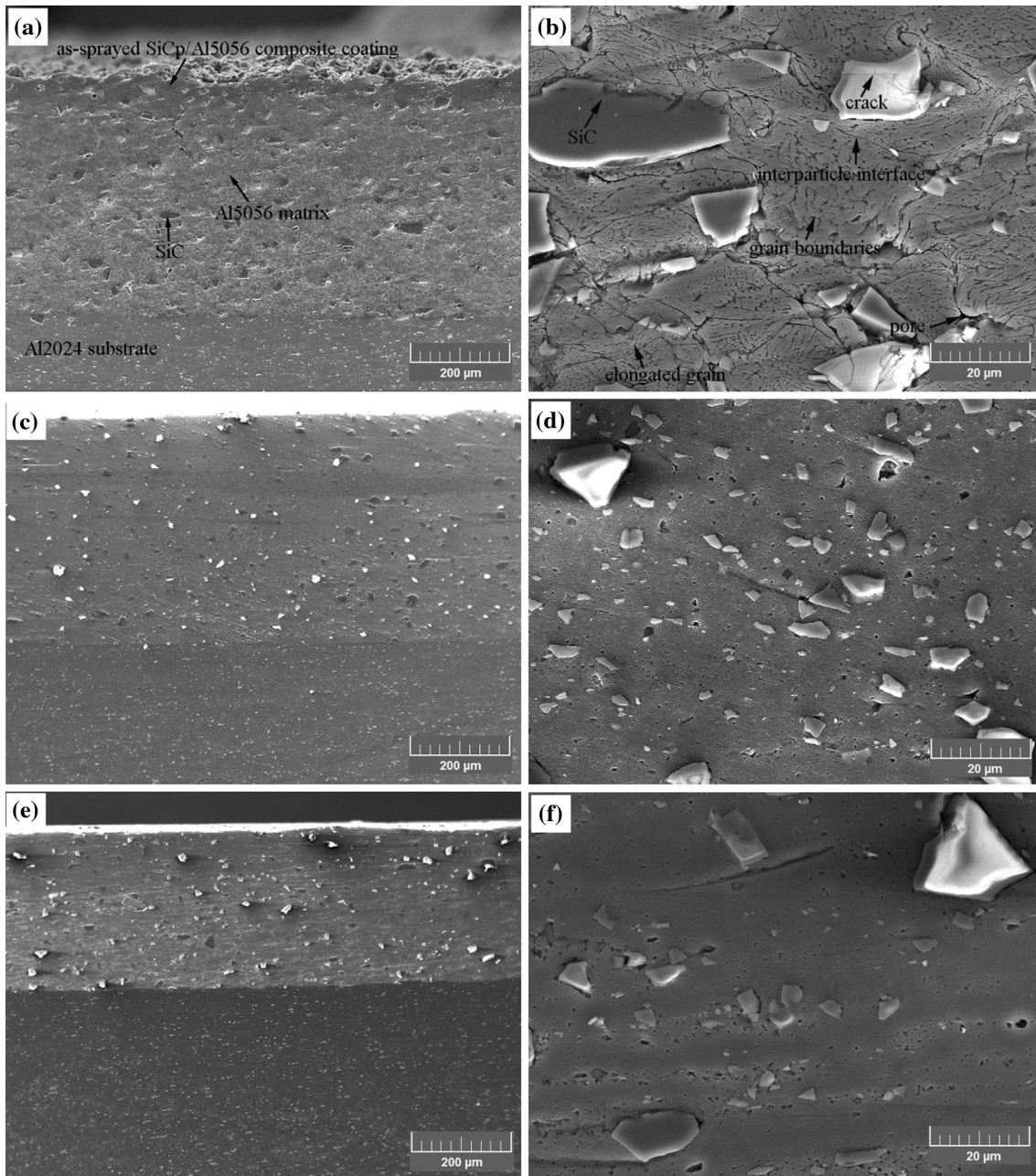


**Fig. 4** Cross-sectional SEM micrographs showing morphology and distribution of SiC particles and Al5056 particles in the coatings: (a) as-sprayed and (b) higher magnification, (c) FSPed at 600 rpm and (d) higher magnification, and (e) FSPed at 1400 rpm and (f) higher magnification

value of 66.9  $\mu\text{m}$  for the starting powder, due to subsequent collisions of SiC particles (Ref 5). While some cracks appeared in large SiC particles, as marked in Fig. 4(b), it can be inferred that such cracking was caused by reflected tension shock waves generated at the impact interface when large SiC particles impinged on previously deposited particles.

Figure 4(c), (e) shows SEM micrographs of central zones of coatings FSPed at rotation speed of 600 and 1400 rpm, respectively, demonstrating the effect of FSP on

the compactness of the coating and the size, morphology, and distribution of particles. It is accepted that tool stirring during FSP causes fragmentation of coarse SiC particles with further dispersion of clustered reinforcement, thus forming a homogeneous distribution of refined SiC particles within the FSPed coating (Ref 7). As shown in Fig. 5(b), (c), the SiC particles in the coating FSPed at 600 rpm presented slightly smaller size (average 6.5  $\mu\text{m}$ ) than in the coating FSPed at 1400 rpm (average 7.0  $\mu\text{m}$ ). However, the coatings showed similar porosity of



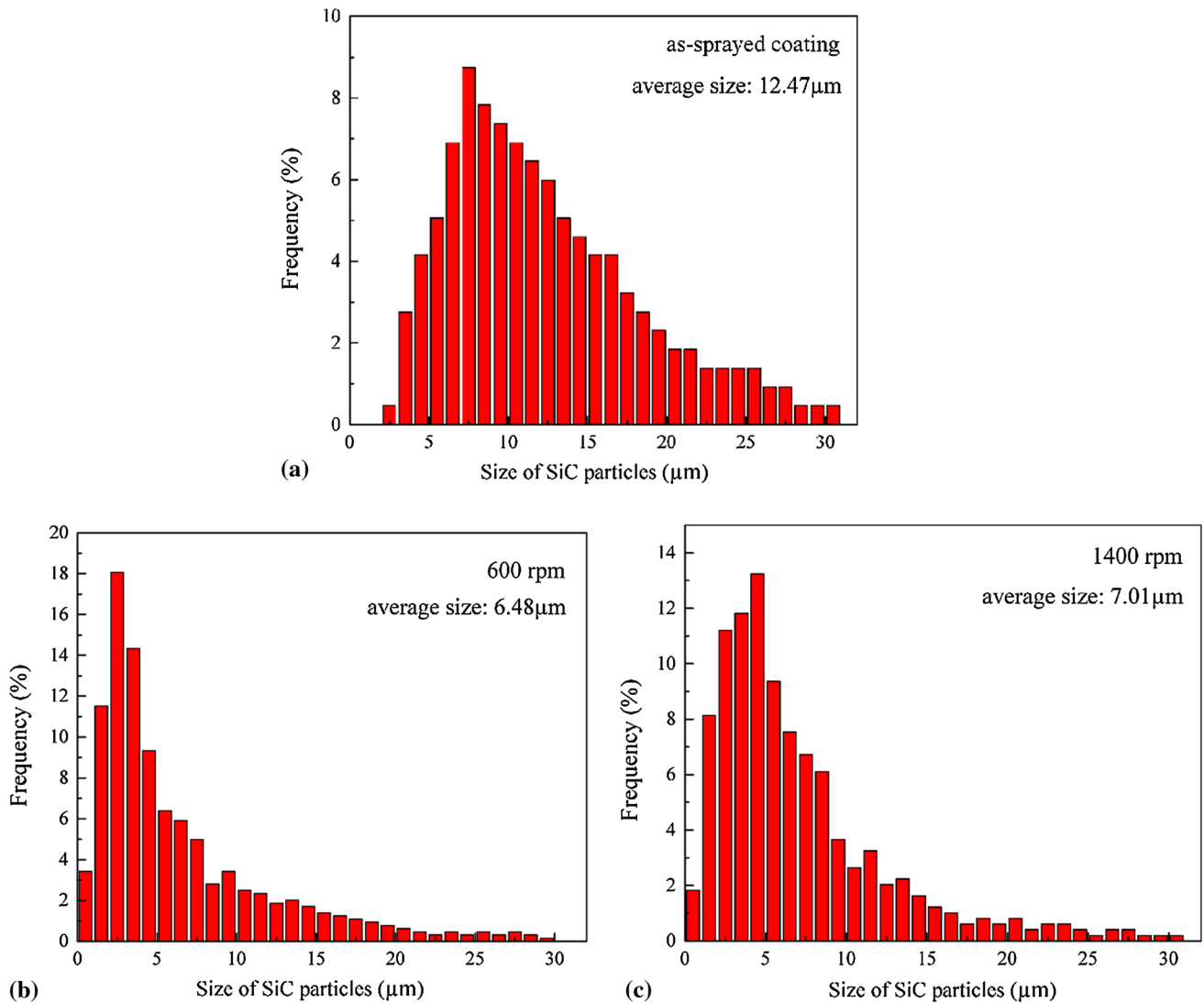


**Fig. 5** Size distribution of SiC particles in coatings: (a) as-sprayed, and FSPed at (b) 600 rpm and (c) 1400 rpm

$0.08 \pm 0.02\%$  for 600 rpm and  $0.09 \pm 0.01\%$  for 1400 rpm, being much lower than for the as-sprayed coating. The porosity increase within FSPed WC-Ni composite coating (Ref 20) could be explained by the fact that the flat cylindrical tool produced insufficient flow of matrix material. Moreover, interparticle interfaces were eliminated after FSP, indicating production of ultrafine grain structure in the Al5056 matrix with strong metal-lurgical bonding at interfaces due to the effect of dynamic recrystallization (Ref 23).

The XRD patterns of the as-sprayed and FSPed coatings are shown in Fig. 6. It is seen that there are almost no new phases, beyond those for the Al5056 matrix and SiC reinforcement. It seems that no reaction occurred between the SiC particles and Al5056 matrix during FSP, and this also demonstrates that FSP is superior to other traditional fusion surfacing techniques such as laser beam and thermal spraying (Ref 22). As reported by many researchers

(Ref 18, 24), undesirable interfacial reactions occur between the matrix and reinforcement during fusion surfacing; For example, Majumdar et al. (Ref 18) detected large Al-carbide phases at SiC/Al interfaces when SiC particles were introduced into Al substrate by laser injection. The reaction product  $Al_4C_3$  is very brittle, degrading the performance of the composite, especially in humid environments. Therefore, the good interfacial condition obtained between the SiC reinforcement and Al5056 matrix during solid-state FSP is beneficial, potentially avoiding unwanted chemical reactions at interfaces.

### 3.3 Microhardness Measurements

The influence of the rotation speed on the coating microhardness is shown in Fig. 7. It can be seen that the average microhardness of the as-sprayed SiCp/Al5056 coating was about 143.9 HV, higher than the values re-

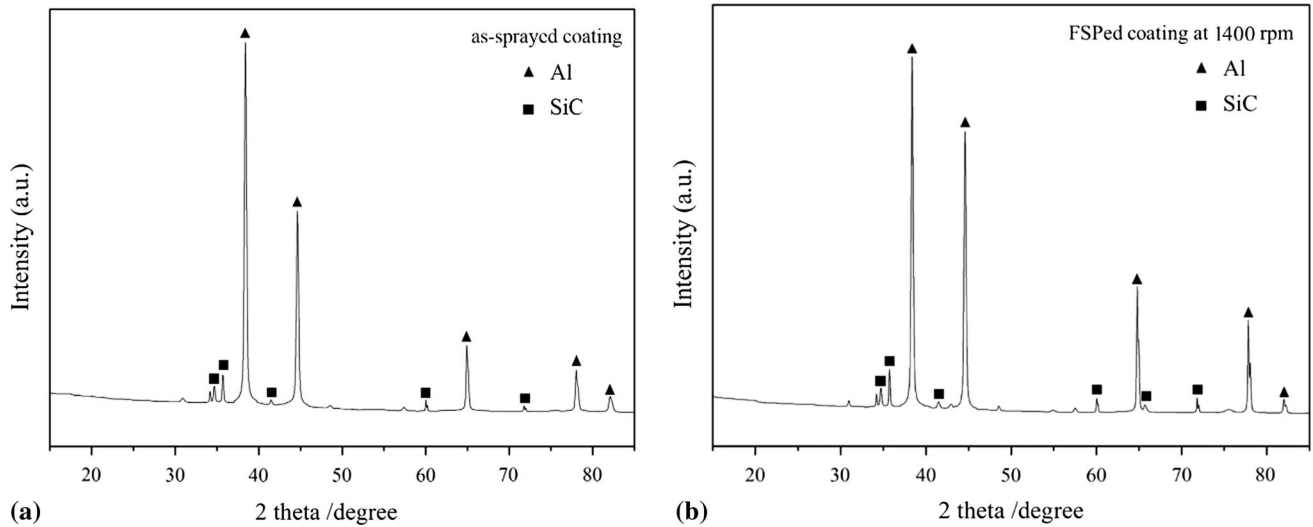


**Fig. 6** XRD patterns of (a) as-sprayed coating and (b) FSPed coating

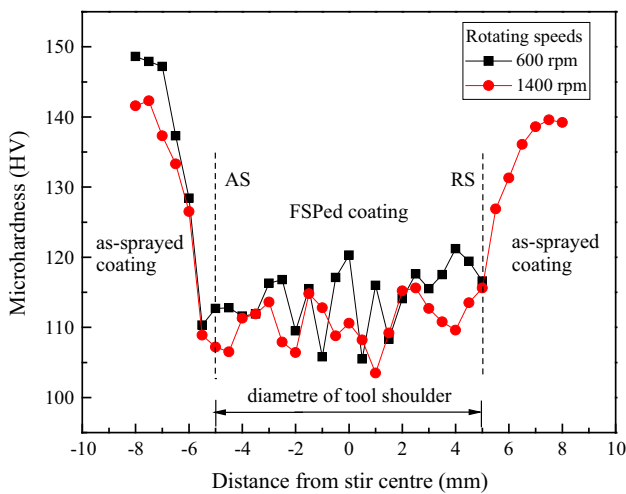


**Fig. 7** Microhardness profiles of coatings FSPed at different rotation speeds

ported for corresponding pure Al alloy coatings by Yu et al. (Ref 5) (Al5056 coating ~111.5 HV). It is known that the non-heat-treatable aluminum alloy Al5056 is strengthened by cold working not precipitation hardening (Ref 18), and this is consistent with the XRD results. The increase of the microhardness can be attributed to two effects: strain hardening, and dispersion strengthening due to the SiC particles. The strain-hardening effect is produced by tamping of subsequent SiC reinforcements on previously deposited Al5056 matrix, through which the Al5056 matrix suffers severe plastic deformation due to the tamping effect (Ref 4, 6, 8). In addition, the dispersion strengthening effect results from the uniformly dispersed SiC particles, which strengthen the matrix by restricting its deformation, thus the as-sprayed coating presents much higher hardness (Ref 25-27). However, the

microhardness profile indicated that application of FSP led to dramatic softening and decrease of the microhardness compared with the as-sprayed coating (from 143.9 HV to about 110 HV), which can possibly be explained based on Fig. 8.

As shown in Fig. 8(a), the interfaces between deposited Al5056 particles exhibit full shear localization due to the supersonic collisions; i.e., where the strains are highest, complicated dislocation-related phenomena, such as dislocation movement, generation, interaction, and accumulation, are involved, leading to formation of subgrains (Ref 28). The higher dislocation density of the composite coating will contribute to strain hardening and increase the microhardness during CS (Ref 6, 29). However, the strain-hardening effect can almost be released for pure coatings after PSHT (Ref 26). Phani et al. (Ref 30) also indicated that that the cold-working effect of a CSed coating can be neglected when it is in a heated state. Application of FSP has dual actions of heat generation and mechanical sweeping of softened metal, and the heat input through friction between the tool and coating leads to softening of the area around the pin (Ref 12, 14). Therefore, it is concluded that, as heat generation and plastic deformation progress, the dislocation processes (i.e., gliding and annihilation) leading to heat production fade as the temperature approaches the melting point, resulting in the decrease of the microhardness. In addition, as revealed in literature, application of FSP generates significant frictional heating and intense plastic deformation, thereby resulting in the occurrence of equiaxed grains (Ref 14, 16, 18, 22, 23) and fine reinforcements (Ref 7, 13, 18, 20) in the stirred zone, as shown in Fig. 8(b). Therefore, the strain-hardened grains are supposed to be replaced with strain-free refined grains. In this case, the strengthening effect of SiC in restricting the deformation of the soft Al matrix is also weakened, leading to a significant decrease of the microhardness (Ref 27). Also, the uniformly dispersed SiC particles strengthen the matrix,

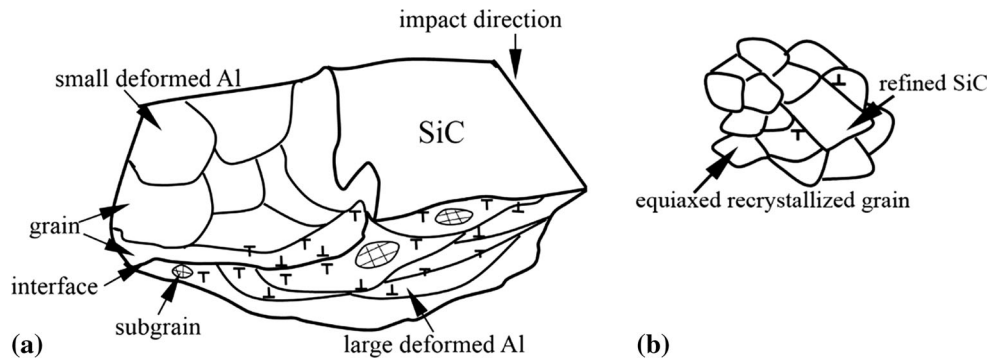


**Fig. 8** Schematics showing proposed mechanism for microstructure formation: (a) as-sprayed coating showing deformed Al particle with dislocation accumulation and formation of subgrains; (b) FSPed coating showing low dislocation density and equiaxed grains

thus the FSPed composite coating still presents relatively high microhardness (Ref 30).

## 4. Conclusions

Increasing the density of a cold-sprayed composite coating, and refining and redistributing the reinforcement, were achieved using FSP with a stir tool characterized by a threaded pin. During FSP, no undesirable interfacial reactions occurred between the matrix and reinforcement, but an obvious reduction of coating thickness (from 665  $\mu\text{m}$  to 632  $\mu\text{m}$  at 600 rpm or 415  $\mu\text{m}$  at 1400 rpm) was observed due to the severe stirring effect. The matrix particles were substantially refined to have ultrafine grains. Meanwhile, finer reinforcement was present, with average size of 6.5  $\mu\text{m}$  for 600 rpm and 7.0  $\mu\text{m}$  for 1400 rpm. FSP changed the bonding mechanism from mechanical to metallurgical bonding between Al5056 particles. Moreover, the microhardness profile of the FSPed coating presented general softening compared with the as-sprayed coating due to release of strain hardening and formation of equiaxed grains. However, the FSPed composite still showed relatively higher microhardness due to the homogeneous distribution of SiC.

## Acknowledgments

C.J. HUANG would like to thank the program of China Scholarship Council (201404490058) and Marie-Curie (268696) for financial support. W.Y. LI would also like to thank the National Natural Science Foundation of China (51574196) and 111 Project (B08040) for support.

## References

1. A. Moridi, S.M. Hassani-Gangaraj, M. Guagliano, and M. Dao, Cold Spray Coating: Review of Material Systems and Future Perspectives, *Surf. Eng.*, 2014, **30**(6), p 369-395
2. W.Y. Li, C.J. Li, and H.L. Liao, Significant Influence of Particle Surface Oxidation on Deposition Efficiency, Interface

- Microstructure and Adhesive Strength of Cold-Sprayed Copper Coatings, *Appl. Surf. Sci.*, 2010, **256**(16), p 4953-4958
3. W.Y. Li, C. Zhang, X.P. Guo, G. Zhang, H.L. Liao, C.J. Li, and C. Coddet, Effect of Standoff Distance on Coating Deposition Characteristics in Cold Spraying, *Mater. Des.*, 2008, **29**(2), p 297-304
4. E. Irissou, J.G. Legoux, B. Arsenaull, and C. Moreau, Investigation of Al-Al<sub>2</sub>O<sub>3</sub> Cold Spray Coating Formation and Properties, *J. Therm. Spray Technol.*, 2007, **16**(5), p 661-668
5. M. Yu, W.Y. Li, X.K. Suo, and H.L. Liao, Effects of Gas Temperature and Ceramic Particle Content on Microstructure and Microhardness of Cold Sprayed SiCp/Al5056 Composite Coatings, *Surf. Coat. Technol.*, 2013, **220**, p 102-106
6. W.Y. Li, C. Yang, and H.L. Liao, Effect of Vacuum Heat Treatment on Microstructure and Microhardness of Cold-Sprayed TiN Particle-Reinforced Al Alloy-Based Composites, *Mater. Des.*, 2011, **32**(1), p 388-394
7. K.J. Hodder, H. Izadi, A.G. McDonald, and A.P. Gerlich, Fabrication of Aluminum-Alumina Metal Matrix Composites via Cold Gas Dynamic Spraying at Low Pressure Followed by Friction Stir Processing, *Mat. Sci. Eng. A*, 2012, **556**, p 114-121
8. Q. Wang, K. Spencer, N. Biribilis, and M.X. Zhang, The Influence of Ceramic Particles on Bond Strength of Cold Spray Composite Coatings on AZ91 Alloy Substrate, *Surf. Coat. Technol.*, 2010, **205**(1), p 50-56
9. W.Y. Li, C. Zhang, H.L. Liao, J.L. Li, and C. Coddet, Characterizations of Cold-Sprayed Nickel-Alumina Composite Coating with Relatively Large Nickel-Coated Alumina Powder, *Surf. Coat. Technol.*, 2008, **202**(19), p 4855-4860
10. W.F. Xu, J.H. Liu, and D.L. Chen, Influence of Test Temperature on the Tensile Properties Along the Thickness in a Friction Stir Welded Aluminum Alloy, *J. Mater. Sci. Technol.*, 2015, **31**(9), p 953-961
11. D.R. Ni, J.J. Wang, and Z.Y. Ma, Shape Memory Effect, Thermal Expansion and Damping Property of Friction Stir Processed NiTi/Al Composite, *J. Mater. Sci. Technol.*, 2016, **32**(2), p 162-166
12. Z.Y. Ma, Friction Stir Processing Technology: A Review, *Metal. Mater. Trans. A*, 2008, **39**(3), p 642-658
13. V. Sharma, U. Prakash, and B.V. Manoj Kumar, Surface Composites by Friction Stir Processing: A Review, *J. Mater. Process. Technol.*, 2015, **224**, p 117-134
14. Z.Y. Ma, R.S. Mishra, and M.W. Mahoney, Superplastic Deformation Behaviour of Friction Stir Processed 7075Al Alloy, *Acta Mater.*, 2002, **50**(17), p 4419-4430
15. A. Kurta, I. Uygurb, and E. Cete, Surface Modification of Aluminium by Friction Stir Processing, *J. Mater. Process. Technol.*, 2011, **211**(3), p 313-317
16. S. Pasebani, I. Charit, and R.S. Mishra, Effect of Tool Rotation Rate on Constituent Particles in a Friction Stir Processed 2024Al Alloy, *Mater. Lett.*, 2015, **160**, p 64-67
17. G.L. You, N.J. Ho, and P.W. Kao, Aluminum Based In Situ Nanocomposite Produced from Al-Mg-CuO Powder Mixture by Using Friction Stir Processing, *Mater. Lett.*, 2013, **100**, p 219-222

18. O.S. Salih, H. Ou, W. Sun, and D.G. McCartney, A Review of Friction Stir Welding of Aluminium Matrix Composites, *Mater. Des.*, 2015, **86**, p 61-71
19. Y. Morisada, H. Fujii, T. Mizuno, G. Abe, T. Nagaoka, and M. Fukusumi, Modification of Thermally Sprayed Cemented Carbide Layer by Friction Stir Processing, *Surf. Coat. Technol.*, 2010, **204**, p 2459-2464
20. H. Ashrafizadeh, A. Lopera-Valle, A. McDonald, and A. Gerlich, in *Effect of Friction-Stir Processing on the Wear Rate of WC-Based MMC Coatings Deposited by Low-Pressure Cold Gas Dynamic Spraying*, Thermal Spray 2015: Proceedings of the International Thermal Spray Conference (Long Beach, CA), 2015, p 41-47
21. C.J. Huang, W.J. Li, Z.H. Zhang, M.S. Fu, M.P. Planche, H.L. Liao, and G. Montavon, Modification of a Cold Sprayed SiCp/Al5056 Composite Coating by Friction Stir Processing, *Surf. Coat. Technol.*, 2016, **296**, p 69-75
22. R.S. Mishra and Z.Y. Ma, Friction Stir Welding and Processing, *Mater. Sci. Eng. R Rep.*, 2005, **50**(1-2), p 1-78
23. Z.H. Zhang, W.Y. Li, J.J. Shen, Y.J. Chao, J.L. Li, and Y.E. Ma, Effect of Backplate Diffusivity on Microstructure and Mechanical Properties of Friction Stir Welded Joints, *Mater. Des.*, 2013, **50**, p 551-557
24. J.D. Majumdar, B.R. Chandra, and I. Manna, Friction and Wear Behavior of Laser Composite Surfaced Aluminium with Silicon Carbide, *Wear*, 2007, **262**, p 641-648
25. A. Shamsipur, S.F. Kashani-Bozorg, and A. Zarei-Hanzaki, The Effects of Friction-Stir Process Parameters on the Fabrication of Ti/SiC Nano-Composite Surface Layer, *Surf. Coat. Technol.*, 2011, **206**(6), p 1372-1381
26. W.Y. Li, C.J. Li, and H.L. Liao, Effect of Annealing Treatment on the Microstructure and Properties of Cold-Sprayed Cu Coating, *J. Therm. Spray Technol.*, 2006, **15**(2), p 206-211
27. O. Meydanoglu, B. Jodoin, and E.S. Kayali, Microstructure, Mechanical Properties and Corrosion Performance of 7075 Al Matrix Ceramic Particle Reinforced Composite Coatings produced by the Cold Gas Dynamic Spraying Process, *Surf. Coat. Technol.*, 2013, **235**, p 108-116
28. Y.S. Tao, T.Y. Xiong, C. Sun, L.Y. Kong, X.Y. Cui, T.F. Li, and G.L. Song, Microstructure and Corrosion Performance of a Cold Sprayed Aluminium Coating on AZ91D Magnesium Alloy, *Corros. Sci.*, 2010, **52**, p 3191-3197
29. K. Kang, G. Bae, J. Won, and C. Lee, Mechanical Property Enhancement of Kinetic Sprayed Al Coatings Reinforced by Multi-walled Carbon Nanotubes, *Acta Mater.*, 2012, **60**, p 5031-5039
30. P.S. Phani, V. Vishnukanthan, and G. Sundararajan, Effect of Heat Treatment on Properties of Cold Sprayed Nanocrystalline Copper Alumina Coatings, *Acta Mater.*, 2007, **55**(14), p 4741-4751